Comparative Study of Reactive and Non-reactive Spark Plasma Sintering Routes for The Production of TaB2-TaC Composites

Melis Kaplan Akarsu
Istanbul Teknik Universitesi
Ipek Akin (akinipe@itu.edu.tr)
Istanbul Technical University https://orcid.org/0000-0002-3159-7650
Filiz Sahin
Istanbul Teknik Universitesi
Gultekin Goller
Istanbul Teknik Universitesi

Research Article

Keywords: TaB2, TaC, Reactive spark plasma sintering, Densification

Posted Date: June 30th, 2021

DOI: https://doi.org/10.21203/rs.3.rs-659977/v1

22 June 2021

Dear Editor,

I am enclosing herewith a manuscript entitled "*Comparative study of reactive and non-reactive spark plasma sintering routes for the production of TaB_2-TaC composites*" for consideration for possible publication in Journal of Advanced Ceramics.

In this study, the influence of reactive spark plasma sintering (RSPS) and non-reactive spark plasma sintering based processing routes on the properties of TaB_2-TaC composites were investigated. Investigations on densification behavior, microstructure, mechanical properties and oxidation behavior of the samples were presented. A near fully dense reactive spark plasma sintered TaB_2 -TaC composite with 6.64 vol% TaC was produced by using Ta_2O_5 and B_4C as reactants.

This study is related with the aims of scope of Journal of Advanced Ceramics in terms of advanced materials processing, structure characterization and properties. Ultra-high temperature ceramics were produced by spark plasma sintering, and then structural characterization and property measurements were conducted.

To the best of our knowledge, this is the first study that investigates the production parameters and mechanical properties of the bulk form of reactively sintered TaB_2-TaC composites.

This manuscript describes original work and is not under consideration by any other journal. All authors have seen and approved the manuscript.

Thank you for receiving our manuscript and considering it for review. I really appreciate your time and look forward to your quick response.

I hope the work is acceptable for publication in Journal of Advanced Ceramics.

Yours sincerely,

Assoc. Prof. Dr. Ipek Akin

Department of Metallurgical and Materials Engineering

Istanbul Technical University

34469 Istanbul, Turkey

Phone: +90 (212) 285 68 95

Email: akinipe@itu.edu.tr

Suggested Referees

1. **Name:** Takashi Goto

   Affiliation: Tohoku University, Institute for Materials Research, 2-1-1 Katahira, Aobaku, Sendai 980-8577, Japan

   Email address: goto@imr.tohoku.ac.jp

2. **Name:** William G. Fahrenholtz

   Affiliation: University of Missouri Rolla, Department of Materials Science and Engineering, 222 McNutt Hall, Rolla, MO 65409, United States

   Email address: billf@umr.edu

3. **Name:** Eugene A. Olevsky

   Affiliation: San Diego State University, 5500 Campanile Dr., San Diego, California, 92182-1323

   Email address: eolevsky@mail.sdsu.edu

The suggested referees' area of expertise is spark plasma sintering (SPS), which is the production method used in this study. Specifically, all referees have extensive works and experience on ultra-high temperature ceramics.

Comparative study of reactive and non-reactive spark plasma sintering routes for the production of TaB_2-TaC composites

Melis Kaplan Akarsu, Ipek Akin*, Filiz Sahin, Gultekin Goller

Istanbul Technical University, Department of Metallurgical and Materials Engineering, Maslak, 34469 Istanbul, Turkey

*Corresponding author. Tel: +90 212 285 6895; fax: +90 212 285 3427

E-mail address: akinipe@itu.edu.tr (I. Akin)

Abstract

The influence of two different spark plasma sintering-based processing routes (i.e., reactive SPS (RSPS) and non-reactive SPS) on the properties of TaB_2-TaC composites was investigated. Ta_2O_5 and B_4C powders were used as starting materials in the RSPS method, and synthesis and densification of TaB_2-TaC composites were accomplished in a facile single step. The effect of sintering temperature and time on the microstructure and densification of the in-situ RSPS were investigated. The obtained results were compared with non-reactive spark plasma sintered TaB_2-TaC composites. The highest densification (~ 99.5 %) was achieved for the TaB_2-TaC composite with 6.64 vol% TaC after reactive sintering at 1550 °C under 40 MPa with a 5 min holding time. Although lower SPS temperature was used in the RSPS method, better densification and higher Vickers hardness were obtained compared to the non-reactive SPS. While platelet-shaped TaC formation was observed in both processes, the average grain size was smaller in the sample produced by the RSPS method. On the other hand, no significant difference was detected in fracture toughness and oxidation behavior of the composites produced by RSPS and non-reactive SPS.

Keywords: TaB_2; TaC; Reactive spark plasma sintering; Densification

1. Introduction

Transition metal borides in groups IVB and VB are members of a family known as ultra-high-temperature ceramics (UHTCs) [1]. The high melting temperatures, excellent chemical stability, high electrical and thermal conductivities, and good corrosion resistance make ultra-high-temperature borides potential candidates for use in extreme chemical and thermal environments [2]. The potential application areas for diborides include the thermal protective structures on the leading-edge components of hypersonic re-entry space vehicles, propulsion systems, furnace elements, refractory crucibles, and plasma-arc electrodes [3]. Various studies

have investigated other borides such as titanium boride (TiB_2), zirconium boride (ZrB_2), and hafnium boride (HfB_2), but tantalum boride (TaB_2) has not been studied widely [1].

TaB_2 is a hard (~20 GPa) UHTC with a melting point of 3037°C and its properties include a density of 11.7 g/cm^3, thermal conductivity of 16 W/m·K, coefficient of thermal expansion of 8.2×10^{-6} K^{-1}, enthalpy of –209 kJ/mol, and free energy of formation of –206.7 kJ at 25°C. TaB_2 has a hexagonal AlB_2 structure and it belongs to the space group of P6/mmm (space number 191). The unit cell contains three atoms with specific positions at (0, 0, 0), and the boron atoms are located at Wyckoff positions of (1/3, 2/3, 1/2) [4]. According to Peshev et al. [5], several methods have been described for the preparation of diborides, including the direct interaction between elements, electrolysis of molten oxides and salts, reducing a mixture of metal oxide and B_2O_3 with carbon, reducing metal oxides with boron carbide under vacuum, and the borothermic reduction of the pure-metal oxides under vacuum. The reactions between oxides and B_4C are endothermic, and they are favorable at temperatures lower than the corresponding carbon reactions [2]. Generally, the B_4C phase is used to promote sintering by removing the residual impurities such as MeO_2 from the surface of MeB_2. You et al. [6] synthesized sub-micrometric TaB_2 powders via the reduction of Ta_2O_5 using B_4C in a mild vacuum (~15 Pa) with starting molar ratios of 1.57 and 1.90 for B_4C/Ta_2O_5. With a molar ratio of 1.57, the reactants were converted into a TaB_2 and B_2O_3 mixture at 1100°C for 2 h. When the molar ratio was fixed and the temperature increased to 1550°C, 38 wt. % TaB_2 and 62 wt. % Ta-rich compounds formed due to the formation of gaseous boron-rich oxides. Guo et al. [7] also investigated the borothermal reduction process for Ta_2O_5 with boron under vacuum where the various borides obtained depended on the molar ratio of boron/Ta_2O_5 and the temperature. Zhang et al. [8] synthesized pure TaB_2 powder by reducing Ta_2O_5 with B_4C and graphite at 1600°C under an argon atmosphere, and then hot pressed with a relative density of ~98% at 2100°C.

Strong covalent bonding and low self-diffusion rates make it difficult to sinter UHTCs [9]. This poor sinterability and the requirement for the high-temperature consolidation of TaB_2-based ceramics limit their applications, where external pressure or an electric field is necessary to overcome this problem. The commonly used techniques for processing UHTCs are pressureless sintering, hot pressing, hot isostatic pressing, and spark plasma sintering (SPS). However, hot pressing and hot isostatic pressing alone are not sufficient to achieve high densification. In addition, unwanted grain growth was reported previously. It is also possible to overcome these

problems by producing composite structures. In the sintering of boride-based UHTCs, various carbides (SiC, TaC etc.) are used as sintering additives to remove the oxide layer on the surface by evaporation-condensation mechanism. It is also known that many carbides added for this purpose lower sintering temperatures by producing eutectic structures. To improve densification of TaB_2, the introduction of small amounts of grain growth inhibitors such as ZrC, TaC, etc. might provide an additional contribution to the densification [10]. Since sintering occurs above 50 % of the melting point, it is also difficult to sinter TaC due to its high melting point of 3880 °C which is the highest for stoichiometric compounds [11]. Zhang et al. [12] reported an enhanced densification for TaC-TaB_2 composite due to physical pinning of grain growth by the second phase addition. Moreover, Demirskyi et al. [13] reported a finer microstructure for the spark plasma sintered TiB_2-TaC composite than that of monolithic TiB_2 and TaC.

The TaC-TaB_2 composites with unique phases and microstructure have advantageous properties in different potential applications [14]. However, the production of dense TaB_2-based ceramics requires both a high processing temperature and high-purity starting powders which are expensive and difficult to obtain. From this point of view, it was aimed to produce TaB_2-TaC composites by facile synthesis at lower sintering temperatures with better densification behavior. TaB_2-TaC composites were produced by RSPS in situ using Ta_2O_5 and B_4C as precursors, which undergo boron carbide reduction reaction and release $B_2O_{3(l)}$. The properties of reactively sintered TaB_2-TaC composites were compared with the non-reactively sintered TaB_2-TaC. The maximum densification behavior associated with RSPS was determined as a criterion for success. This is the first study that investigates the production parameters and mechanical properties of the bulk form of reactively sintered TaB_2-TaC composites.

2. Materials and methods

The starting materials were commercially available Ta_2O_5 (99.99%, Inframat, USA), B_4C (Grade HS, H.C. Starck Corp., Germany), TaB_2 (99%, American Elements, USA), and TaC (99.7%, Inframat, USA) respectively. The average particle sizes of the starting Ta_2O_5, B_4C, TaB_2, and TaC powders were measured as ~39.5 µm, ~1.78 µm, ~45 µm, and ~2.3µm, respectively, using a laser particle size analyzer (Malvern Mastersizer 2000). The starting powders of RSPSed composites were prepared from a molar ratio of 1.57 for B_4C/Ta_2O_5. Powders were ball milled in a polythene bottle with SiC balls in ethanol for 24 h. A magnetic stirrer was applied for 5 h to disperse the powders well before evaporating the ethanol. The powder mixture was dried in an oven at 100 °C for 24 h. The mixture was then pounded in an

agate mortar to obtain a soft and non-agglomerated starting powder. A cylindrical graphite die with a diameter of 50 mm was used for the sintering process. The entire contact zone of the powder on the punches and die was covered with a graphite sheet to ensure better conductivity. Sintering was conducted using an SPS apparatus (7.40 MK-VII, SPS Syntex Inc.). A pulsed direct current (12 ms/on, 2 ms/off) was applied throughout the entire SPS process under a vacuum atmosphere. A blank run was used (with the sintering conditions) to determine the effects of the thermal expansion of the graphite die and punches. The sintering temperature, time, and pressure were summarized in Table 1. The heating rate of 100 °C/min was used in all experiments. The sample names were coded for clarity, where RS, P, and C corresponds to reactive sintering, ready to press powder, and composite structure. The numbers designated the experimental order (Table 1). During experiments, the die temperature was measured and controlled using an optical pyrometer (Chino, IR–AH), which was focused on a small hole in the graphite die. The sintering process was conducted in the temperature-controlled mode while monitoring the shrinkage behavior of the specimens.

The sintered samples were ground with diamond disks before obtaining the density measurements. The Archimedes method was used to determine the density of the sintered samples where distilled water was employed as the immersion medium. The theoretical density was calculated with the rule of mixtures based on TaB_2 and TaC contents. The relative density of the TaB_2 -TaC composites was determined by the ratio of bulk density and theoretical density. The phase compositions of the samples were determined by XRD (MiniFlex, Rigaku Corp.) in the 2θ range 20°–80° at a scanning rate of 2°/min with CuKα radiation. The Rietveld refinement of X-ray diffraction data was used to determine the relative amounts of the phases. The lattice parameter a for cubic TaC was calculated by Eq. (1) to determine the y in the TaC_y [15].

$$a(y) = 4.3007 + 0.1563y \quad (1)$$

Microstructural analyses were conducted on the fractured surfaces using a scanning electron microscope (SEM, JSM 7000 F, JEOL). Before SEM analysis, the sintered samples were polished to remove the graphite sheet and coated with gold by sputtering. The compositional analysis was carried out using energy dispersive X-ray spectroscopy (EDS, JEOL 5410, Noran 2100). The microhardness of the samples was measured using a microhardness tester (VHMOT, Leica Corp.) fitted with a Vickers indenter. The samples were ground and polished before obtaining the measurements. Indentations were produced on the polished surfaces under a load

of 9.8 N. The indentation fracture toughness of each sample was calculated using the Anstis equation [16] based on the half-length of the crack formed around the indentations under a load of 19.6 N. Thermogravimetric (TG) analysis was performed in air using a TG/DTA analyzer (PerkinElmer Diamond TG DTA). The samples were heated from 25 °C to 1100 °C at a heating rate of 5 °C/min.

3. Results and discussion

3.1. Densification behavior and phase analysis

In this study, RSPSed composites were produced using Ta_2O_5 and B_4C as precursors, which undergo a solid-state reaction that leads to pore formation. Thus, it was approached to the densification process of RSPSed composites in three stages: formation of TaB_2 and TaC phases, densification, and elimination of pores. In the standard state, Ta_2O_5 and B_4C reactions are favorable above 85 ℃ based on Eq. (2). However, due to more negativity in Gibbs free energy, Eq. (3) is much easier to occur because it is favorable at all temperatures. In the standard state, Eq. (4) also becomes favorable above 1436 ℃ [6]. According to Eq. (3), reaction products are $TaB_{2(s)}$, $TaC_{(s)}$, and $B_2O_{3(l)}$, and enthalpy of mixing of the compounds can be sorted as $B_2O_{3(l)}$< $TaC_{(s)}$< $TaB_{2(s)}$. The formation tendency of B_2O_3 is higher than that of TaC and TaB_2 due to high negativity.

$$7Ta_2O_{5(s)} + 11B_4C_{(s)} \rightarrow 14TaB_{2(s)} + 8B_2O_{3(l)} + 11CO_{(g)} \quad (2)$$

$$9Ta_2O_{5(s)} + 11B_4C_{(s)} \rightarrow 7TaB_{2(s)} + 11TaC_{(s)} + 15B_2O_{3(l)} \quad (3)$$

$$7TaC_{(s)} + 2B_4C_{(s)} + 3B_2O_{3(l)} \rightarrow 7TaB_{2(s)} + 9CO_{(g)} \quad (4)$$

Table 1 shows the relative densities and volume fractions of the reactive and non-reactive (PC-1) sintered TaB_2 -TaC composites. It was observed that the sintering parameters had different effects on the obtained phase ratios and density results. Only TaB_2 and TaC phase formation was obtained in all RSPSed and SPSed samples. According to Rietveld analysis (Table 1), in the reactive SPS process, it was determined that the volume fraction of TaB_2 increased from ~82.1% for RSC-1 to ~93.3% for RSC-3 with an increase in reactive SPS temperature under 40 MPa with a holding time of 5 min. The bulk and relative densities of the samples also increased with an increase in reactive SPS temperature.

Table 1 Sintering parameters, relative density, and quantitative phase analyses of sintered TaB_2-TaC composites obtained from the Rietveld refinement method based on their XRD patterns (SPS pressure is 40 MPa. Theoretical densities of TaB_2 and TaC are 11.7 g/cm^3 and 14.3 g/cm^3, respectively.)

Sample	SPS Temperature (°C)	Holding Time (min)	TaB_2 (vol%)	TaC (vol%)	Bulk Density (g/cm^3)	Relative Density (%)
RSC-1	1250	5	82.14	17.86	4.96	40.77
RSC-2	1350	5	84.77	15.23	9.21	76.14
RSC-3	1550	5	93.36	6.64	11.82	99.55
RSC-4	1550	10	91.67	8.33	9.78	82.07
RSC-5	1550	15	89.96	10.04	5.40	45.14
PC-1	1550	5	93.36	6.64	10.35	87.26

The best densification was achieved in RSC-3 (~99.5%). The sintering process was conducted by both Eqs. (3) and (4) that proved based on the sintering temperature and C/Ta ratio of RSC-3. The residual impurity removal by the B_4C phase could be the main factor that provides the highest densification. Yuan et al. [17] have reported that B_2O_3 has a high vapor pressure in the temperature range used to densify ZrB_2 ascribe to the removal of B_2O_3 by evaporation on the surface of ZrB_2 powder. Herein, the removal of B_2O_3 by evaporation from the surface of TaB_2 could be another reason for the improved densification of RSC-3. A significant decrease in oxygen by the evaporation of B_2O_3 at 1500 °C was reported previously [17]. Moreover, Zhang et al. [18] calculated the ΔG°_{rxn} for vaporization of B_2O_3 (given in Eqs. (5) and (6)):

$$B_2O_{3(l)} \rightarrow B_2O_{3(g)} \quad (5)$$

$$\Delta G^{\circ}_{rxn} = 368314 - 157.85T(J) \quad (6)$$

Corresponding to the grain rearrangement due to the formation of a liquid phase, vaporization of B_2O_3 enhanced the densification of TaB_2, and the volume fraction of TaB_2 increased in consequence of reaction as ~ 11 % in the RSPSed composite structure. To investigate the effect of liquid phase formation on densification behavior, ready-to-sinter TaB_2 and TaC powders were consolidated by SPS with the same composition (6.64 vol% TaC) and same process parameters with RSC-3. It was observed that the sintered composite (PC-1) only achieved ~87.2 % relative density (Table 1). An increase in SPS temperature from 1550 to 1800 °C (not given) slightly increased the density (~4.3%), whereas the density of RSC-3 was even higher. Furthermore, only 90 % relative density was achieved for monolithic TaB_2 after sintering at

1750 °C under 40 MPa with a 5 min holding time. The densification behavior of the reactive (RSC-3) and non-reactive (PC-1) sintered TaB_2-TaC composites was evaluated using the displacement curves shown in Fig. 1. The shrinkage starting temperatures of non-reactive sintered PC-1 was 1280 ℃. The shrinkage for RSC-3 and PC-1 finished at 1510 ℃. Two specific temperatures were detected for the accelerated shrinkage at ~980 and ~1350 °C for reactive sintered RSC-3. The first temperature (~980 °C) corresponded to the beginning of the conversion of the reactants to the products according to Eq. (3). The second shrinkage (at ~1350 °C) could be attributed to the gas release from the system as a consequence of Eq. (5). The displacement curves of RSC-3 supported the effective sintering of the liquid phase formation. In addition, the two-step shrinkage behavior of the RSC-3 provided better densification than that of PC-1. Different mechanisms of reaction during RSPS could be possible explanations of such behavior. The sharp sample displacement of the synthesis promoted product densification [19].

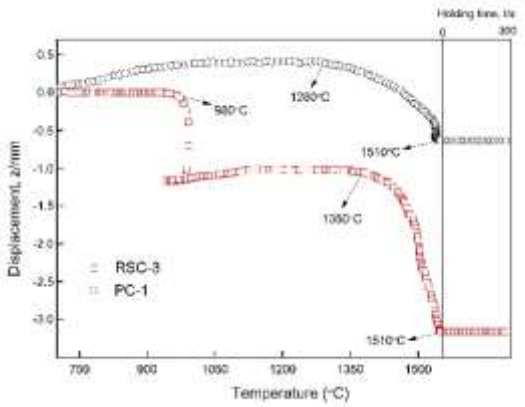

Fig. 1 Displacement curves of RSC-3 and PC-1.

In contrast to change in SPS temperature, longer holding time at 1550 °C led to a significant decrease in the relative density of TaB_2 -TaC composites (Table 1). B_2O_3 phase boils above 1405.6 ℃ when no other gases were present, otherwise if CO presents, it suppresses B_2O_3 pressure and lowers the boiling point [17]. The increase in holding time negatively affected the densification due to the complete transformation of $B_2O_{3(l)}$ to $B_2O_{3(g)}$. A more liquid phase may have transformed into a gas phase during a longer holding time at 1550 °C. Therefore, a certain amount of porosity forms in RSC-4 and RSC-5 samples as a consequence of B_2O_3 evaporation [17,20]. The action of evaporation of B_2O_3 caused porosities in the structure and a longer holding time promoted the formation of a higher amount of TaC [8]. The quantitative phase analyses of sintered samples obtained from the Rietveld refinement method based on their XRD

patterns revealed that the volume fraction of TaC increased when the holding time increased from 5 min to 10 and 15 mins. The volume fraction of TaC increased from ~6.6 to ~8.3 and ~10.0 vol% for RSC-3, RSC-4 and RSC-5, respectively, with an increase in holding time at 1550 °C under 40 MPa. The favorability of equation (3) under vacuum could be the reason for the higher amount of TaC through the reaction [8]. The high negativity in the enthalpy of the mixing of TaC makes it more favorable than TaB_2. Also, the fast carbon diffusion, which is a characteristic feature of SPS could be another reason. Demirskyi et al. [21] reported that an increased carbon diffusion rate could be beneficial if the layered carbon structures are required in the final structure. Although a higher amount of TaC phase formed in RSC-4 and RSC-5, the remained porosities due to evaporation of B_2O_3 caused lower bulk density.

Considering the high amount of gas released as a consequence of the RSPS, herein sintering temperature was limited up to 1550 °C. Strong exothermic reactions in the formation of TaB_2 lead to several inconveniences. B_2O_3 and CO gases produced are not allowed to escape from the confined environment (graphite die/punches) during RSPS that revealed safety problems, especially during the combustion regime synthesis reactions [10].

The XRD patterns of reactive spark plasma sintered composites are shown in Fig. 2. The XRD patterns of all the reactive sintered composites contained the characteristic peaks of TaB_2 (JCPDS 03-065-3385) and $TaC_{0.95}$ (JCPDS 03-065-8145). The liquid B_2O_3 phase was not identified in the XRD pattern of the samples due to its amorphous nature. The carbon amount in the TaC_y was calculated using Eq. (1) as 0.9954 and 0.9849 for RSC-3 and PC-1, respectively (Table 2). The XRD patterns of PC-1 before and after sintering are shown in Fig. 3. The XRD patterns of sintered PC-1 contained the same characteristic peaks of phases as RSC-3. Although PC-1 contains TaC as a starting powder, the $TaC_{0.95}$ phase was detected after sintering at 1550 °C. The XRD peaks of TaC phases shifted to lower angles after sintering at 1550° C, which indicated enlargement of TaC lattice. Previously, Liu et al. [22] reported that the various impurities in the starting powders can incorporate into TaC lattice as a consequence of reaction. Accordingly, C/Ta ratio changes could be attributed to the oxide impurities of TaB_2 powder (the oxygen impurity information provided by the supplier is 0.32 wt.%). The oxide impurities can be removed by the presence of TaC. In addition, the C/Ta ratio was affected by C loss that forms CO (Eq. (4)) [23]. None of the RSPS samples denoted peak shift, which corresponds to solid solubility. TaB_2-TaC system components are virtually insoluble in each other up to 2100°C [24]. Owing to the difference in the crystal structure of hexagonal TaB_2 (AlB_2 type) and cubic TaC (B1), TaB_2 is insoluble in TaC [12]. The peak intensity of the TaC phase

decreased with increasing SPS temperature (Fig. 2a-c), which is consistent with the SEM images of the samples (Fig.4). Increasing SPS temperature decreased the amount of TaC platelets and their thickness (Fig.4b and d).

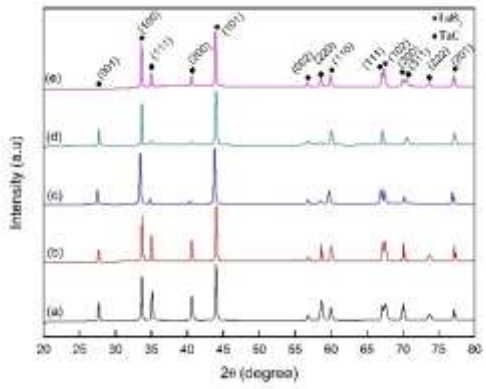

Fig. 2 XRD patterns of reactive sintered TaB_2-TaC composites a) RSC-1, b) RSC-2, c) RSC-3, d) RSC-4, and e) RSC-5.

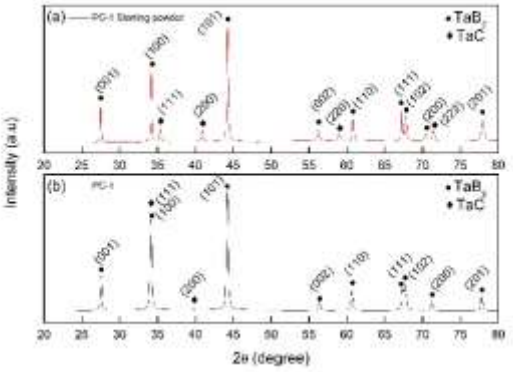

Fig. 3 XRD patterns of PC-1 a) before sintering, and b) after sintering.

3.2. Microstructural characterization

SEM images of the fracture surfaces of reactive and non-reactive sintered TaB_2-TaC composites are shown in Fig.4. Microstructural investigations and EDS analysis of the samples supported the XRD results. Neck formation between TaB_2 grains (Fig. 4b) in RSC-2 was detected after reactive sintering at 1350 ℃. A previous study reported that the evaporation temperature of B_2O_3 is above 1300°C [25]. Porosities formed in RSC-2 as a consequence of the rapid evaporation of the liquid B_2O_3 during reactive sintering. In addition, slight grain coarsening of TaB_2 was observed in RSC-2 (Fig.4b). TaC grains became more visible and took place in the boundaries of the TaB_2 grains (indicated by yellow circles in Fig. 4b). At 1550 ℃, an almost fully dense TaB_2 -TaC composite (RSC-3) with residual porosity in the order of ~ 0.5 % was

achieved with grain coarsening (Fig.4c and d). The formation of more uniform TaB_2 grains was observed in RSC-3. Both rounded shape TaB_2 and TaC platelets were detected in the microstructure for all reactive (Fig.4c and d) and non-reactive (Fig. 4f) sintered composites. TaC grains were located at the grain boundaries (indicated by yellow circles in Fig. 4d). In addition, fracture surface SEM images of monolithic TaB_2 were given in Fig.S1 in the ESM. No secondary phase or TaC formation was observed due to carbon diffusion after the sintering process of monolithic TaB_2 at 1750 °C. Microstructural investigations of the fracture surface of the monolithic sintered TaB_2 support the ~10% porosity measured in the structures. Most of the pores were detected in the triple junction points of the grains (Fig.S1b in the ESM). Fig. S1c and d in the ESM also show the fracture surface of the TaB_2-TaC composite sintered at 1800 °C. Similar to PC-1, TaC platelets were located at the grain boundaries of the TaB_2 grains.

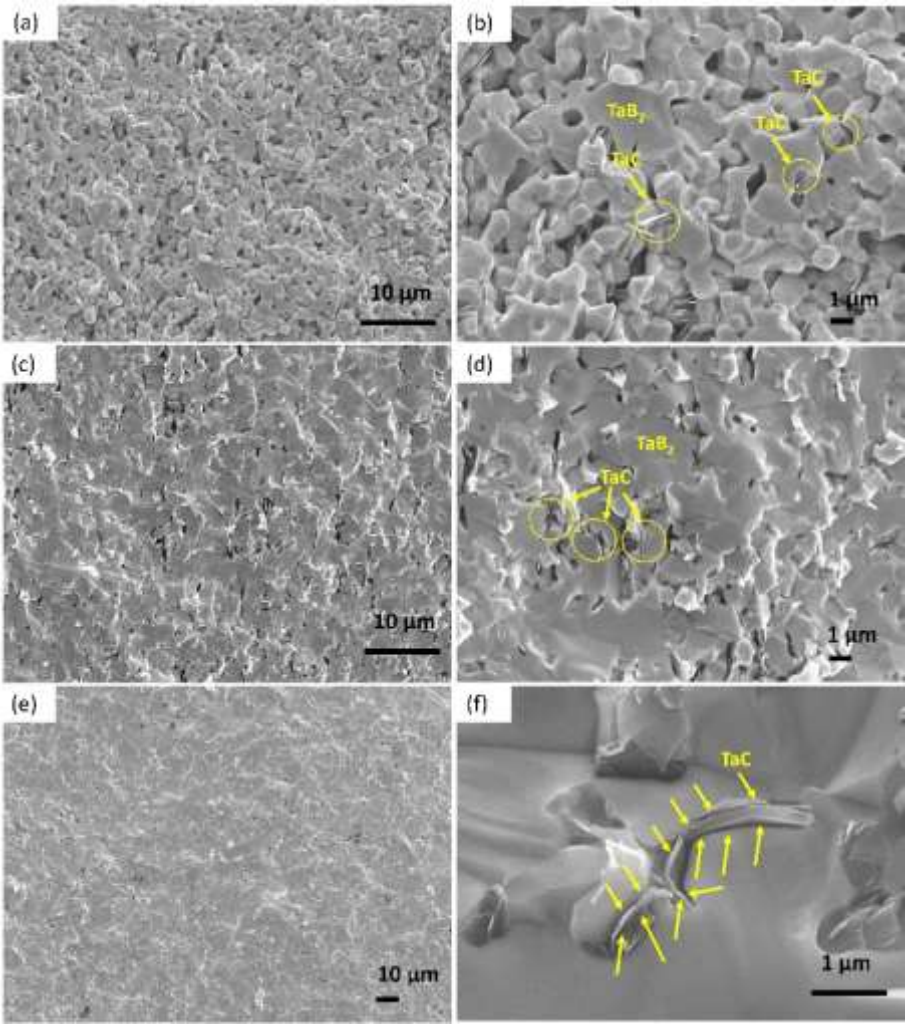

Fig. 4 Fracture surface micrographs of TaB_2-TaC composites (a) RSC-2 (x2k), (b) RSC-2 (x5k), (c) RSC-3 (x2k), (d) RSC-3 (x5k), (e) PC-1 (x550), and (f) PC-1 (x20k).

EDS analysis was performed to investigate the composition of the TaC phase in RSC-5. EDS spectrum of the grain (indicated by the yellow dot in Fig. 5a) was shown in Fig. 5b. EDS analysis determined the composition of 56.3% Ta and 43.6% C (in at.%).

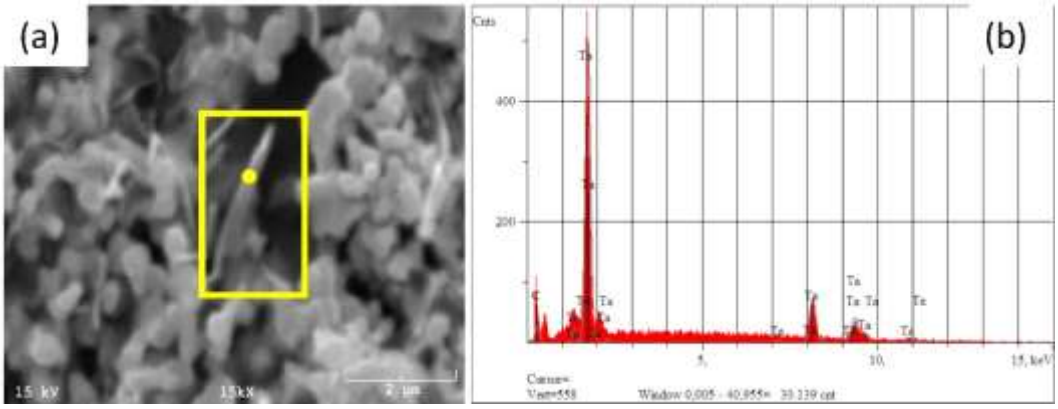

Fig. 5 (a) Fracture surface micrograph of RSC-5, and b) EDS analysis of TaC platelet from the yellow dot.

The changes in the C/Ta ratio have an impact on the morphology of TaC grains. Namely, equiaxed grains are formed in the single-phase TaC. Nevertheless, changes in the C/Ta ratio resulted in either equiaxed grains with secondary-phase laths in a crisscross pattern or acicular grains were reported [26]. The opportunity to produce different morphologies by phase content regulates mechanical properties such as tensile strength, creep, and fracture toughness. [27]. Previously, Zhao et al. [28] produced in-situ growth TaC whiskers toughened Al_2O_3 ceramic matrix composites in two steps: (1) production of in-situ TaC whiskers in Al_2O_3 powder that includes raw powders as Ta_2O_5 and carbon black for the synthesis of TaC whiskers, and (2) hot pressing the composite. The authors reported an improvement in the mechanical properties of Al_2O_3 matrix composite by the toughening effects (such as crack deflection, interface debonding, whisker fracture, and whisker pullout) of TaC particles and whiskers. Herein, the C/Ta ratio of both RSPSed and SPSed samples was less than 1. Thus, platelet-like TaC grains were obtained instead of equiaxed grains. Similarly, increasing the sub-stoichiometric C/Ta ratio enhanced the fracture toughness.

The non-reactive sintered PC-1 displayed a coarser microstructure (Fig. 4f and Fig. 6d) than that of RSC-3. The larger grain size of TaB_2 and TaC could be another reason for the lower densification of PC-1. The grain sizes of TaC in RSC-3 and PC-1 were in the range between 0.5-1 µm and 0.7-1.8 µm, respectively. Talmy et al. [29] reported that the grain size of TaC is a strong function of carbon stoichiometry, and sub-stoichiometric TaC increased the average

grain size. C/Ta ratio of PC-1 (0.9849) was less than that of RSC-3 (0.9954); therefore, due to higher sub-stoichiometry of PC-1, TaC grains were much bigger than that of RSC-3. This result is consistent with the observations of previous studies [13] that transition metal carbides of group VB exhibited rapid grain growth during high temperature SPS.

Increasing the holding time from 5 to 15 min decreased the relative density of the samples. The decline in the relative density from ~99.5% to ~45.1% could be related to the levels of porosity according to the SEM images (Fig.6). Longer holding time produces more TaC phase due to the evaporation of B_2O_3 (Table 1), which was also detected in Fig.6. From Fig. 6a to c, while the amount of TaC and porosity increase in the microstructure, the amount of TaB_2 decreases, and the microstructure become finer.

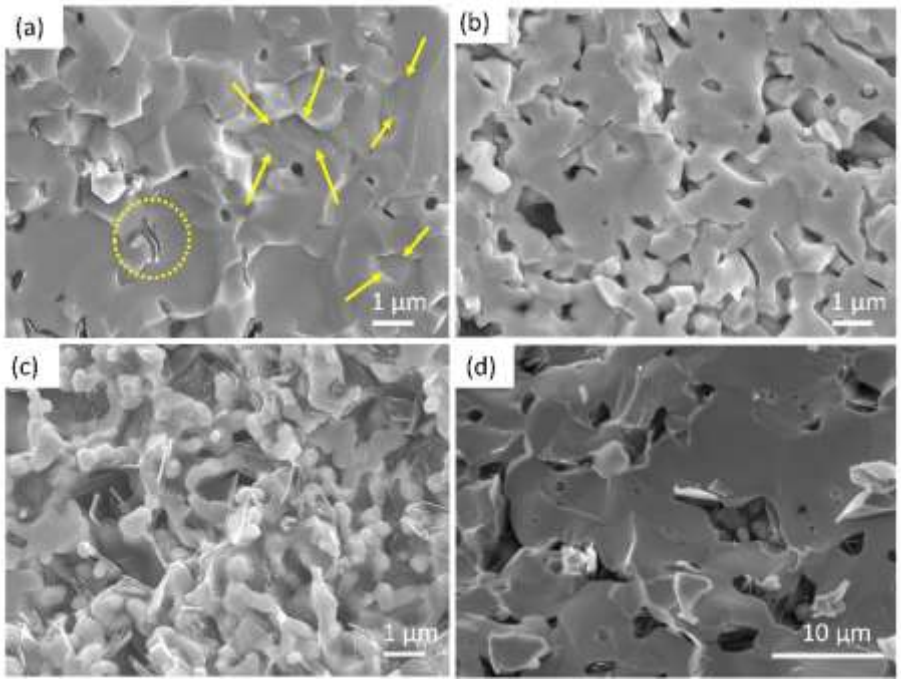

Fig. 6 Fracture surface micrographs of (a) RSC-3, (b) RSC-4, (c) RSC-5and (d) PC-1.

3.4. Mechanical properties

The mechanical properties of RSC-3 and PC-1 were evaluated. The average Vickers hardness values were obtained as ~18.1 and ~16.5 GPa for RSC-3 and PC-1, respectively (Table 2). Vickers hardness of monolithic sintered TaB_2 was ~19 GPa. Previously, Vickers hardness of the spark plasma sintered TaB_2 (~ 96% relative density) was reported as ~25 GPa [30]. The relative density and average Vickers hardness were reported as ~94.6% and ~18 GPa, and ~94% and ~14 GPa for reactive spark plasma sintered TaB_2 [10] and hot-pressed TaC [12], respectively. Moreover, Vickers hardness of the spark plasma sintered TaC-11 wt% TaB_2

composite (~ 95.8% relative density) was reported as ~21.8 GPa [23]. The hardness of the RSC-3 is compatible with RSPSed monolithic TaB_2, monolithic TaC, and composites structures. Also, owing to RSPS, the process temperature was lowered to 1550 °C, which is quite below the sintering temperature of the aforementioned studies. This is the first study on TaC reinforcement to TaB_2 matrix. Thus, mechanical properties were not reported previously. Poor densification with ~ 13% porosity and large grain size in the PC-1 could be the reason for the lower hardness.

Table 2 Vickers hardness, indentation fracture toughness, and C/Ta ratio of the RSC-3 and PC-1.

	C/Ta ratio	Vickers hardness (GPa)	Fracture toughness ($MPa \cdot m^{1/2}$)
RSC-3	0.9954	18.1±0.52	3.84±0.22
PC-1	0.9849	16.5±0.34	3.94±0.25

Indentation fracture toughness was calculated based on the crack length in the Vickers indentations by using a volumetric rule of mixtures for a composite containing TaB_2 (E=551 GPa) [8] and TaC (E=537 GPa) [31]. In this study, indentation fracture toughness was calculated as ~3.84 and ~3.94 $MPa \cdot m^{1/2}$ for RSC-3 and PC-1, respectively (Table 2). In the previous studies, fracture toughness was reported as ~4.7 $MPa \cdot m^{1/2}$ for TaB_2, based on the reactive sintering of Ta and 2B [32], ~3.5 $MPa \cdot m^{1/2}$ (94 % relative density) for hot-pressed TaC [12], and ~3.4 $MPa \cdot m^{1/2}$ (98.6 % relative density) for hot-pressed TaC-10 wt% TaB_2 composite [12]. The fracture toughness of the PC-1 was slightly higher than that of RSC-3. This could be related to the larger size of TaC platelets in PC-1, as explained in section 3.3. Fracture toughness of ~3.3 $MPa \cdot m^{1/2}$ was obtained for monolithic sintered TaB_2. Although PC-1 had better fracture toughness than that of monolithic sintered TaB_2, it is slightly lower than that of some previously reported values for monolithic TaB_2. This situation could be attributed to the agglomeration of TaC platelets (indicated by the dotted yellow circle in Fig. 6a) and the fracture mode of the composite structure. The combination of intergranular and transgranular fracture modes was detected in RSC-3. In addition, cleavage planes (indicated by yellow arrows in Fig. 6a) were detected in the fracture surface, which is characteristic of the brittle transgranular fracture mode. Demirskyi et al. [21] stated that when the monolithic TaB_2 specimens were approaching full densification, the majority of the specimens were fractured in intergranular mode and weaker bonding between grains was observed. Moreover, Zhang et al. [33] reported intergranular fracture mode for TaC, and both intergranular and transgranular fracture modes for TaC with

B_4C additions. The authors reported that intragranular fracture did not result in a higher strength for multiphase TaC, owing to the thermal expansion coefficient mismatch that causes tensile or compressive stress near two-phase boundaries.

3.4. TG analysis

The oxidation behavior of the samples was examined using TGA up to 1100 °C at a heating rate of 5 °C/min. All samples retained their structural integrity after the oxidation tests. The variation in the mass as a function of temperature is shown in Fig. 7. Weight gains of 1.74% and 1.50% were obtained for RSC-3 and PC-1, respectively. The fact that the PC-1 mass gain is lower than that of RSC-3 may be ascribed to the relative density difference. Although no significant difference was detected between mass gains of RSC-3 and PC-1, oxidation paths were different. The change of RSC-3 tends to increase exponentially. A mass loss was observed for PC-1 up to ~ 500 °C. The weight started to increase at ~ 600 °C for RSC-3 and ~ 500 °C for PC-1. The oxidation of TaB_2 and TaC starts at ~ 600 °C and 400 °C, respectively [34,35]. Both composites exhibited passive oxidation behavior that formed a protective oxide film on the surface according to oxidation of TaB_2. Desmasion-Brut et al. [36] reported that TaC does not form an oxide layer. A carbon diffusion occurred from the center to the surface of the sample that limits the oxide layer formation. Even if the oxide film forms it is not protective due to the evolution of gaseous products [37]. TaB_2 and TaC oxidize according to Eqs. (7) and (8) [36,38]:

$$2TaB_{2(s)} + 11/2O_{2(g)} \rightarrow Ta_2O_{5(s)} + 2B_2O_{3(l)} \quad (7)$$

$$2TaC_{(s)} + 9/2O_{2(g)} \rightarrow Ta_2O_{5(s)} + 2CO_{2(g)} \quad (8)$$

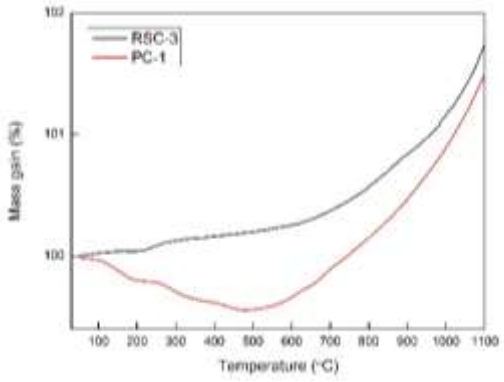

Fig. 7 Mass gain in the air for RSC-3 and PC-1.

4. Conclusions

A near fully dense reactive spark plasma sintered TaB_2-TaC composite with 6.64 vol% TaC was produced by using Ta_2O_5 and B_4C as reactants. To investigate the effect of the sintering route, ready-to-press TaB_2 and TaC powders were sintered using the same process parameters. However, similar densification was not achieved. The characterization of the composites revealed that reactively sintered TaB_2-TaC composite exhibited better densification and higher hardness than that of non-reactively sintered composite. While platelet-shaped TaC formation was observed in both processes, the average grain size was smaller in the reactive sintering method. No significant difference was detected in fracture toughness and oxidation behavior of the composites produced by reactive and non-reactive SPS. Overall, good mechanical properties and high densification at low process temperature make the reactively sintered TaB_2-TaC composites potential candidates for use in ultra-high temperature applications.

Acknowledgment

This work was supported by Istanbul Technical University [grant number MGA-2017-40907]. The authors are thankful to Huseyin Sezer, Can Burak Danisman, and Baris Yavas for microstructural investigations, and SPS experiments, respectively.

Electronic Supplementary Material

Supplementary material (Fig. S1) is available in the online version of this article.

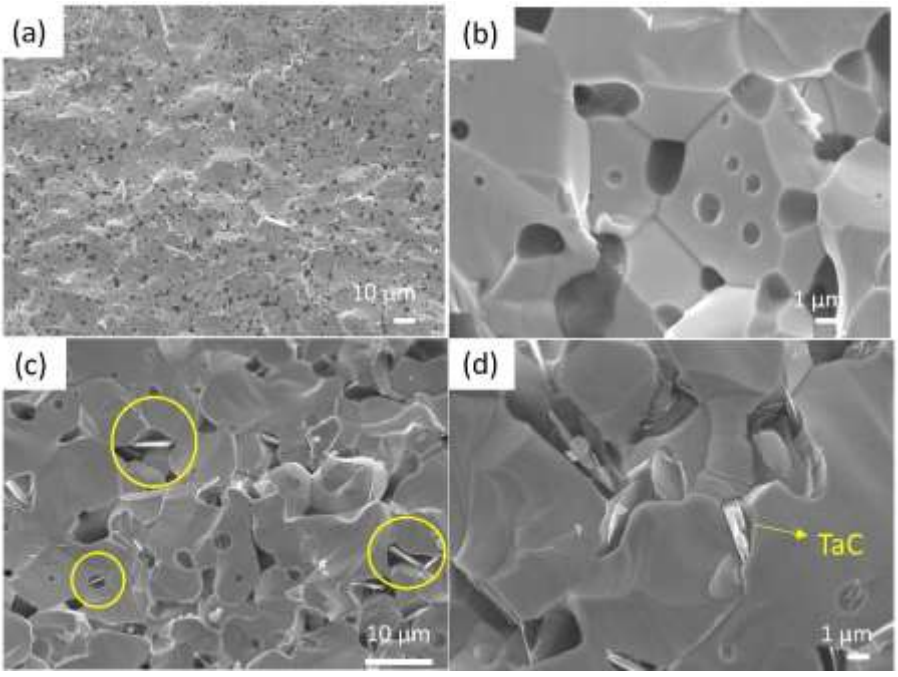

Fig. S1 Fracture surface micrographs of (a-b) monolithic TaB_2 and (c-d) non-reactive SPSed TaB_2-TaC composite.

References

[1] Yeh CL, Wang HJ. A comparative study on combustion synthesis of Ta-B compounds. *Ceram Int* 2011, **37**: 1569–73.

[2] Fahrenholtz WG, Hilmas GE, Talmy IG, Zaykoski JA. Refractory diborides of zirconium and hafnium. *J Am Ceram Soc* 2007, **90**: 1347–64.

[3] Guo SQ. Densification of ZrB2-based composites and their mechanical and physical properties: A review. *J Eur Ceram Soc* 2009, **29**: 995–1011.

[4] Fahrenholtz WG, Wuchina EJ, Lee WE, Zhou Y. Ultra-high temperature ceramics: Materials for extreme environment applications. New York, Wiley, 2013

[5] Peshev P, Leyarovska L, Bliznakov G. On the borothermic preparation of some vanadium, niobium and tantalum borides. *J Less-Common Met* 1968, **15**: 259–67.

[6] You Y, Tan DW, Guo WM, Wu SH, Lin HT, Luo Z. TaB2 powders synthesis by reduction of Ta2O5 with B4C. *Ceram Int* 2017, **43**: 897–900.

[7] Guo W-M, Zeng L-Y, Su G-K, Li H, Lin H-T, Wu S-H. Synthesis of TaB2 powders by borothermal reduction. *J Am Ceram Soc* 2017, **100**: 2368–72.

[8] Zhang X, Hilmas GE, Fahrenholtz WG. Synthesis, densification, and mechanical properties of TaB2. *Mater Lett* 2008, **62**: 4251–3.

[9] Sciti D, Silvestroni L, Medri V, Monteverde F. Sintering and densification of ultra-high temperature ceramics. *Ultra-High Temp Ceram Mater Extrem Environ App.* 2014, 112–43.

[10] Licheri R, Musa C, Orrù R, Cao G, Sciti D, Silvestroni L. Bulk monolithic zirconium and tantalum diborides by reactive and non-reactive spark plasma sintering. *J Alloys Compd* 2016, **663**: 351–9.

[11] Khaleghi E, Lin Y, Meyers A, Olevsky EA. Spark plasma sintering of tantalum carbide. *Scr Mater* 2010, **63**: 577–80.

[12] Zhang X, Hilmas GE, Fahrenholtz WG. Densification, mechanical properties, and oxidation resistance of TaC–TaB2 ceramics. *J Am Ceram Soc* 2008, **91**: 4129–32.

[13] Demirskyi D, Sakka Y. High-temperature reaction consolidation of TaC-TiB2 ceramic composites by spark-plasma sintering. *J Eur Ceram Soc* 2015, **35**: 405–10.

[14] OuYang X, Yin F, Hu J, Liu Y, Long Z. Thermodynamic modeling of B-Ta and B-C-Ta systems. *J Phase Equilibria Diffus* 2017, **38**: 874–86.

[15] Bowman AL. The variation of lattice parameter with carbon content of tantalum carbide. *J Phys Chem* 1961, **65**: 1596–8.

[16] Anstis GR, Chantikul P, Lawn BR, Marshall DB. A critical evaluation of indentation techniques for measuring fracture toughness: I Direct crack measurements. *J Am Ceram Soc* 1981, **46**: 533–8.

[17] Yuan H, Li J, Shen Q, Zhang L. In situ synthesis and sintering of ZrB2 porous ceramics by the spark plasma sintering –reactive synthesis (SPS–RS) method. *Int J Refract Met Hard Mater* 2012, **34**: 3–7.

[18] Zhang S, Hilmas GE, Fahrenholtz WG. Pressureless densification of zirconium diboride with boron carbide additions. *J Am Ceram Soc* 2006, **89**: 1544–50.

[19] Orrù R, Cao G. Comparison of reactive and non-reactive spark plasma sintering routes for the fabrication of monolithic and composite Ultra High Temperature Ceramics (UHTC) materials. *Materials* 2013, **6**: 1566–83.

[20] Yuan H, Li J, Shen Q, Zhang L. Preparation and thermal conductivity characterization of ZrB2 porous ceramics fabricated by spark plasma sintering. *Int J Refract Met Hard Mater* 2013, **36**: 225–31.

[21] Demirskyi D, Vasylkiv O. Consolidation and grain growth of tantalum diboride during spark plasma sintering. *Ceram Int* 2016, **42**: 16396–400.

[22] Liu H, Liu L, Ye F, Zhang Z, Zhou Y. Microstructure and mechanical properties of the spark plasma sintered TaC/SiC composites: Effects of sintering temperatures. *J Eur Ceram Soc* 2012, **32**: 3617–25.

[23] Liu L, Ye F, He X, Zhou Y. Densification process of TaC/TaB2composite in spark plasma sintering. *Mater Chem Phys* 2011, **126**: 459–62.

[24] Ordan'yan SS, Unrod VI, Polishchuk VS, Storonkina NM. Reactions in the system TaC-TaB2. *Powder Metall Met Ceram* 1976, **15**: 692–5.

[25] Jung EY, Kim JH, Jung SH, Choi SC. Synthesis of ZrB2 powders by carbothermal and borothermal reduction. *J Alloys Compd* 2012, **538**: 164–8.

[26] Morris RA, Wang B, Matson LE, Thompson GB. Microstructural formations and phase transformation pathways in hot isostatically pressed tantalum carbides. *Acta Mater* 2012, **60**: 139–48.

[27] Thompson GB, Weinberger CR. Tantalum carbides: Their microstructures and deformation behavior. In: Fahrenholtz WG, Wuchina E., Lee W., Zhou Y, editors. *Ultra-High Temp Ceram Mater Extrem Environ Appl.* 2014: 291–315.

[28] Zhao G, Huang C, Liu H, Zou B, Zhu H, Wang J. Preparation of in-situ growth TaC whiskers toughening Al2O 3 ceramic matrix composite. *Int J Refract Met Hard Mater* 2013, **36**: 122–5.

[29] Talmy IG, Zaykoski JA, Opeka MM. Synthesis, processing and properties of TaC-TaB2-C ceramics. *J Eur Ceram Soc* 2010, **30**: 2253–63.

[30] Musa C, Orrù R, Licheri R, Cao G. Spark plasma synthesis and densification of TaB2 by pulsed electric current sintering. *Mater Lett* 2011, **65**: 3080–2.

[31] Brown HL, Armstrong PE, Kempter CP. Elastic properties of some polycrystalline transition metal monocarbides. *J Chem Phys* 2012, **45**: 547–9.

[32] Laszkiewicz-Łukasik J, Jaworska L, Putyra P, Klimczyk P, Garzeł G. The influence of SPS heating rates on the synthesis reaction of tantalum diboride. *Bol la Soc Esp Ceram y Vidr* 2016, **55**: 159–68.

[33] Zhang X, Hilmas GE, Fahrenholtz WG. Densification and mechanical properties of TaC-based ceramics. *Mater Sci Eng A* 2009, **501**: 37–43.

[34] Matsushita J, Hwang GC, Shim KB. Oxidation behavior of tantalum boride ceramics. *Solid State Phenom* 2007, **126**: 819–22.

[35] Nisar A, Ariharan S, Venkateswaran T, Sreenivas N, Balani K. Oxidation studies on TaC based ultra-high temperature ceramic composites under plasma arc jet exposure. *Corros* 2016, **109**: 50-61

[36] Alexandre N, Desmaison J. Comparison of the oxidation behaviour of two dense hot isostatically pressed tantalum carbide (TaC and Ta2C) materials. *J Eur Ceram Soc* 1997, **17**: 1325–34.

[37] Zhang C. High temperature oxidation study of tantalum carbide-hafnium carbide solid solutions synthesized by spark plasma sintering. *FIU Electronic Theses and Dissertations*. 2016; 2985.

[38] Silvestroni L, Guicciardi S, Melandri C, Sciti D. TaB2-based ceramics: Microstructure, mechanical properties and oxidation resistance. *J Eur Ceram Soc* 2012, **32**: 97–105.

Supplementary Files

This is a list of supplementary files associated with this preprint. Click to download.

- FigS1.jpg